Available online at www.sciencedirect.com

ScienceDirect

Nuclear Physics A 978 (2018) 160–172

NUCLEAR PHYSICS A

www.elsevier.com/locate/nuclphysa

Excitation functions of the $p + {}^{93}$Nb reaction in the energy range 10–22 MeV

Siddharth Parashari [a,*], S. Mukherjee [a,*], B.K. Nayak [b], R. Makwana [a], S.V. Suryanarayana [b], H. Naik [c], S.C. Sharma [b]

[a] *Department of Physics, Faculty of Science, The M. S. University of Baroda, Vadodara-390002, India*
[b] *Radiochemistry Division, Bhabha Atomic Research Center, Mumbai-400085, India*
[c] *Nuclear Physics Division, Bhabha Atomic Research Center, Mumbai-400085, India*

Received 26 June 2018; received in revised form 1 August 2018; accepted 1 August 2018
Available online 3 August 2018

Abstract

Excitation functions of the proton induced reactions on ^{93}Nb were measured using the stack foil activation followed by off-line γ-ray spectrometry at 14UD BARC-TIFR Pelletron accelerator, Mumbai, India. Proton beam of 22 MeV was used for the present analysis and was degraded along the stack of five niobium foils. We have identified ^{93m}Mo, ^{92m}Nb and ^{89g}Zr reaction residues populated through (p, n), (p, pn) and $(p, \alpha n)$ reaction channels, respectively. The measured cross-section data were compared with the existing literature data available in EXFOR and were found to be in a good agreement. The calculated excitation functions were also compared with the theoretical predictions of TALYS-1.9 code using suitable input parameters for the pure compound nucleus (CN) and pre-equilibrium (PE) reaction cross-sections. The PE process was found to be dominant over the CN process at higher incident proton energies. The present work is also essential for the production cross-section and dose estimation for the medical isotope ^{89g}Zr in PET diagnostics procedure.

Keywords: ^{93}Nb$(p, n)^{93m}$Mo; ^{93}Nb$(p, pn)^{92m}$Nb and ^{93}Nb$(p, \alpha n)^{89g}$Zr reactions; Off-line γ-ray spectrometry; TALYS-1.9; Pre-equilibrium emission

* Corresponding authors.
E-mail addresses: siddharthparashri5@gmail.com (S. Parashari), sk.mukherjee-phy@msubaroda.ac.in (S. Mukherjee).

https://doi.org/10.1016/j.nuclphysa.2018.08.002
0375-9474/

1. Introduction

Niobium is the least dense metal among the refractory metals and still has various uses. It possesses high strength, high melting point, and can be worked through annealing to achieve a wide range of elasticity. It has a great importance in modern space, aircraft and nuclear reactor technology [1]. Niobium has broad applications as a superconducting material. Together with Tin (Sn), it is used in the toroidal coils of the International Thermonuclear Experimental Reactor (ITER) [2]. Different alloys of niobium are capable of generating strong magnetic fields, and therefore, they are used as wires for the superconducting magnets and the nuclear magnetic resonance instruments in linear and small medical accelerators. Due to the essential refractory properties of niobium, it is a valuable constituent in ADSs, and hence, the charged particle induced reaction cross-sections of niobium become vital for the accelerator technology. On the other hand, the excitation function of the proton-induced reaction cross-sections are also of interest for the production yields of ^{89}Zr due to its medical and biological uses.

A notable amount of data have been reported over the years for the proton-induced reaction cross-sections with niobium metal using different measurement techniques. It can be stated from the EXFOR [3] compilation that the literature data has a significant uncertainty and the reported cross-sections from different authors [4–13] also have minor discrepancies. The disagreement of the literature data over the wide range of incident proton energies is possibly due to the relative measurement of reaction cross-sections with the different monitor reactions. Single charged particle induced reactions at such higher energies can be carried out by the compound nucleus mechanism, however, several experimental evidences [14–18] suggests that there is a finite probability of particle emission before the compound nucleus sets into the statistical equilibrium. A similar kind of attempt has been made [19] to understand the energy dependence of pre-equilibrium (PE) emission for niobium up to 12 MeV. The geometry dependent hybrid model proposed by Blann [20,21] has been found thriving in reproducing the light-ion induced experimental data using the model code ALICE-91 [22]. On the other hand, the comparison of experimental data with a much-updated code TALYS-1.8 was shown in recent work by Lawriniang et al. [23]. The authors had successfully reproduced the experimental ^{93}Nb$(p,n)^{92m}$Mo reaction cross-sections data by modifying the input optical model potential parameter. However, the modification was not found to be the unique as it could not reproduce the ^{93}Nb$(p,pn)^{93m}$Nb reaction cross-sections.

Taking this as the sole motivation for the present work, we have studied the excitation function for the proton-induced niobium reactions using off-line activation technique. The flux was measured directly from the Faraday cup and by monitoring the current. The technique is helpful in order to make the masured cross-sections independent of monitor reaction cross-sections, which enables us to minimize the uncertainty in the data. The experimentally produced data were compared with the theoretical data from TALYS-1.9 code [24]. Different level density models have also been tested for the present case in order to find the best-suited model among all. The data measured in the present work would be useful for the accelerator technology, for optimizing a radioisotope production and also for verification of different models to better understand the dependence of PE emission on the Q-value of the different reactions.

2. Experimental methodology

The measurement of excitation functions for the present experiment was carried out by using the stack foil activation technique [25,26] followed by off-line γ-ray spectroscopy at 14UD

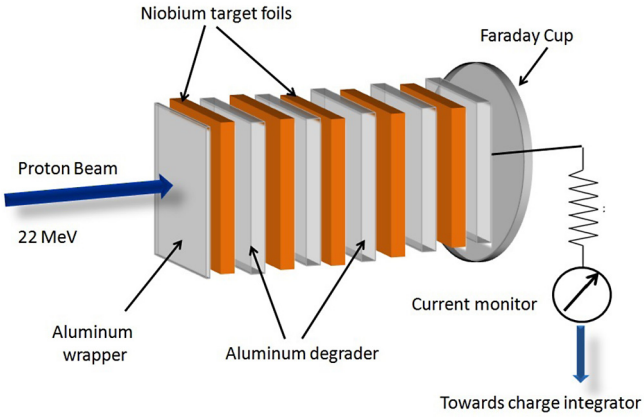

Fig. 1. (Color online.) The schematic diagram of the experimental setup at 14UD BARC-TIFR Pelletron accelerator.

Bhabha Atomic Research Centre – Tata Institute of Fundamental Research (BARC-TIFR) Pelletron facility in Mumbai, India. High purity ($\approx 99.98\%$) Niobium foils of thickness ≈ 22 μm and area 1 cm^2 were used as target. Aluminum foils of appropriate thickness were applied after each Nb target foil to reduce the beam energy significantly in steps of about 2 MeV per target. The proton energy degradation along the stack was calculated by SRIM code [27]. A schematic diagram of the stack is presented in Fig. 1. The stack wrapped in thin aluminum foil was kept inside the 6 meter irradiation port, just before the analyzing magnets on the main beam line of the Pelletron. This port is most suitable for the irradiation experiments which require high proton flux.

The energy spread for the proton beam at 6 meter height beamline was 50–90 keV. At this port, the terminal voltage was regulated by generating voltage mode (GVM) using the terminal potential stabilizer. A thick Ta collimator of 6 mm diameter was used to get a proper circular shaped beam. The stack was irradiated inside a Faraday cup holder at a constant 160 nA proton current for about 1.5–2.0 hours to build up sufficient activity. The proton flux during the irradiation was calculated from the charge collected on a Faraday cup and using current as well. The irradiated samples were allowed to cool for about four hours to reduce the radioactive dose before recording the γ-ray spectra. Each sample was counted by using a pre-calibrated 80 cm^3 single crystal HPGe detector coupled to a PC based multi channel analyzer. The irradiated samples were placed at a distance of 5 cm from the detector end cap to avoid the summing effect and to reduce the dead time of the detector. The HPGe detector was calibrated with a standard ^{152}Eu source. The resolution of the detector system during counting was measured as 1.82 keV at 1332 keV of ^{60}Co. Each irradiated Nb sample was counted for about 1 hour to minimize the counting statistic uncertainty. The counting of the samples was repeated over a period according to the decay half-life of the reaction products. Fig. 2 shows a 78 hours cooled spectrum from Nb foil irradiated at 19 MeV proton energy. The characteristic γ-lines with their respective half-lives were used to identify the residual nuclei of interest like ^{93m}Mo, ^{92m}Nb, and ^{89g}Zr. The detector efficiency for the 1477.14 keV γ-line was determined by extrapolating the polynomial fit of the energy vs efficiency curve. A typical efficiency curve measured at a distance of 5 cm from the detector head is shown in Fig. 3. The spectroscopic data used in the present calculations were taken from the NuDat [28] database, whereas the Q-values and the threshold energies were taken from Qtool [29], which are summarized in Table 1.

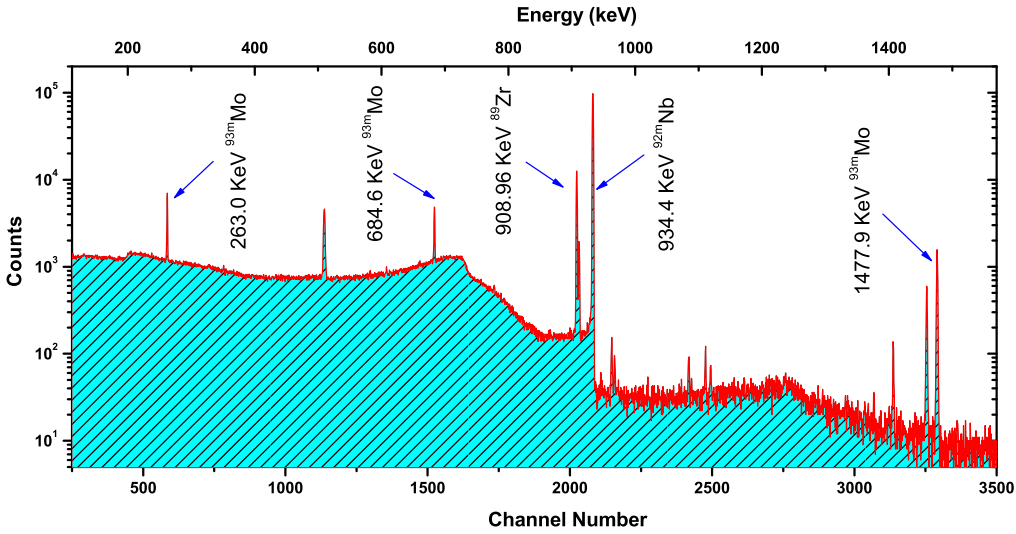

Fig. 2. (Color online.) The typical γ-ray energy spectrum obtained from the interaction of $p + {}^{93}$Nb at $E_{Lab} \approx 19$ MeV.

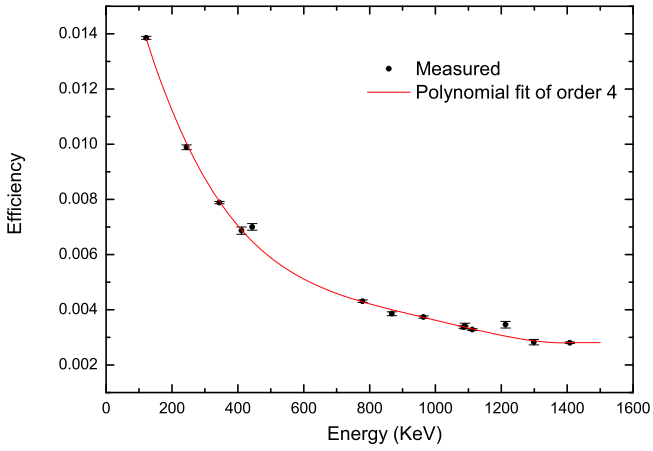

Fig. 3. (Color online.) The measured efficiency with the ^{152}Eu source keeping at 5 cm from the detector head.

3. Data analysis

The excitation function of the proton induced reaction on ^{93}Nb was calculated at five energies within the range 10–22 MeV. The mid-point energy for each Nb foil was calculated by SRIM code [27] and were found to be 21.85 ± 0.14, 19.53 ± 0.16, 16.98 ± 0.17, 14.13 ± 0.20 and 11.56 ± 0.23 MeV, respectively. At such high incident proton energies, several reaction channels populate and result in different residues. In the present case of study, we have identified three residues, ^{93m}Mo, ^{92m}Nb, and ^{89g}Zr, populated through (p, n), (p, pn) and $(p, \alpha n)$ reaction channels, respectively. All these residues were identified using the spectroscopic properties of their characteristic gamma lines [28] and by following their half-lives [28] from different counting statistic data. The radionuclide ^{93}Mo has ground state with a half-life of 4.0×10^3 years

Table 1
List of the identified residues in the $p + {}^{93}$Nb reaction with their spectroscopic data [28,29].

Nuclide	$T_{1/2}$	Deacy mode	E_γ (keV)	I_γ (%)	Channel	E_{Th} (MeV)
^{93m}Mo	6.85 ± 0.07 h	IT (99.88 %)	263.05 ± 0.13	57.40 ± 0.11	(p, n)	1.20
		ϵ(0.12%)	684.69 ± 0.21	99.9 ± 0.8		
			1477.14 ± 0.03	99.10 ± 0.11		
^{93g}Mo	$(4.0 \pm 0.8) \times 10^3$ y	ϵ(100%)	–	–	–	–
^{92m}Nb	10.15 ± 0.02 d	ϵ(100%)	934.44 ± 0.10	99.15	(p, pn)	9.06
^{92g}Nb	$(3.47 \pm 0.24) \times 10^7$ y	ϵ(100%)	934.5	74.0 ± 0.11		
		$\beta^+ (< 0.05\%)$				
^{89m}Zr	4.16 ± 0.10 min	IT(93.77%)	587.83 ± 0.01	89.62	$(p, \alpha n)$	5.60
^{89g}Zr	78.41 ± 0.12 h	ϵ(100%)	909.15 ± 0.15	99.14		

and a metastable state (^{93m}Mo) with a comparably short half-life of 6.85 hours. The γ-lines of 263.05 keV (57.4%), 684.69 keV (99.8%) and 1477.14 keV (99.1%) were used to evaluate the cross-sections for the metastable state of ^{93m}Mo. However, the metastable state ^{92m}Nb has a half-life of 10.15 hours, which is very short as compared to its ground state ($T_{1/2} = 3.47$ years). It prevents the intermixing of events coming from the common γ-line of both the ground as well as the metastable state. Therefore, the spectrum recorded after a short cooling time was used for the estimation of cross-sections by identifying 934.44 keV (99.15%) gamma line. The radionuclide ^{89}Zr also possesses both ground and metastable states with half-lives of 78.41 hours and 4.18 min respectively. Therefore, in this case, we have identified only ^{89}Zr by using 909.15 keV (100%) γ-line. The photopeak counts from each γ-lines described above were used to calculate the reaction cross-sections for each residue using the following formula [30],

$$\sigma_R = \frac{C_{obs}\lambda(\frac{CL}{LT})}{N_0\phi I_\gamma K\epsilon(1-e^{-\lambda t_i})(e^{-\lambda t_c})(1-e^{-\lambda LT})} \quad (1)$$

where σ_R is the reaction cross-section, C_{obs} is the photo peak count of the γ-line of interest, C_L and L_T are the clock time and the live time for the counting of the spectrum, λ is the decay constant, I_γ is the branching ratio for the each γ-ray taken from Ref. [28], N_o is the total number of the target nuclei in the sample, ϵ is the detector efficiency, ϕ is the proton flux and $K = [1 - exp(-\mu d)]/(\mu d)$ is the correction factor for the self absorption of the γ-rays in the sample thickness 'd' with absorption coefficient μ.

4. Experimental results

In the present work, the excitation function of the ^{93}Nb$(p, n)^{93m}$Mo, ^{93}Nb$(p, pn)^{92m}$Nb and ^{93}Nb$(p, \alpha n)^{89g}$Zr reactions have been measured at five proton energies of 21.85 ± 0.14, 19.53 ± 0.16, 16.98 ± 0.17, 14.13 ± 0.20 and 11.56 ± 0.23 MeV, respectively. The experimental cross-section for all the residues are summarized in Table 2. The present cross-sections were also compared with the literature data available in EXFOR [3] and the theoretical model code TALYS-1.9 [24]. The uncertainties in the present measurements were obtained as the quadratic sum of both statistical and systematic uncertainties. As the primary source, the statistical error in the present measurement was estimated to be $< 5\%$. The statistical uncertainty was reduced by performing the counting of each sample for a significant time. There could be various sources for the systematic uncertainty in the measured cross-sections. The fluctuations in the beam current may result in the uncertainty in the incident flux. The current was kept constant during the

irradiation, and the error due to the flux is estimated to be $< 2\%$. The estimation of the foil thickness may lead to the uncertainty in determining the number of target nuclei and comes out to be $< 3\%$. An uncertainty may appear due to the solid-angle effect, as the irradiated samples were not point-source like the ^{152}Eu standard source but had a finite diameter, and it is found to be $< 2\%$. The dead time of the HPGe detector was kept $< 1.5\%$ by adjusting the sample to detector distance. The overall errors in the present measurements have been estimated to be $< 10\%$.

4.1. Theoretical cross-section calculations using the TALYS-1.9 model code

The TALYS-1.9 [24] is the most updated theoretical model code that is being used worldwide for nuclear data prediction for light particle induced reactions for the energies up to 200 MeV. The TALYS model code uses the reaction parameters from the RIPL database [31]. The code accounts for the effect of level density parameters, compound, pre-equilibrium, and direct reaction mechanisms as a function of the incident particle energy. The optical model parameters were obtained by using a global potential, proposed by Koning and Delaroche [32]. The compound nucleus reaction mechanism have been incorporated by using the Hauser–Feshbach model [33]. The pre-equilibrium contribution have been accounted an exciton model which was developed by Kalbach [34]. In the present work, the experimental data were compared with the cross-sections reproduced by activating different level density models (ldmodel 1-6) present in the TALYS-1.9 [24]. The different level densities used (ldmodel 1-6) account for, constant temperature Fermi gas model (CTFGM) [35], Back-shifted Fermi gas model (BSFGM) [36], Generalized superfluid model (GSFM) [37,38], Microscopic level densities from Goriely's and Hilaire's tables [39] and Microscopic level densities (temperature dependent HFB, Gogny force) [40], respectively. It was well evident from the recent work by Lawriniang et al. [23] that the default TALYS-1.8 values were unable to reproduce the experimental data beyond a certain point. Therefore, all the level density parameters were tested for the three reaction residues, and the results are plotted in Fig. 4–6 along with the present experimental results as well as the data taken from EXFOR [3]. The experimental data for the ^{93}Nb$(p,n)^{93m}$Mo reaction is plotted in Fig. 4. It can be seen that the CTFGM (ldmodel 1) was in good agreement with the results up to 17 MeV proton energies; however, above this energy region the theoretical values from any of the level density models were not able to fit the experimental results. Similarly, in the case of ^{93}Nb$(p,pn)^{92m}$Nb reaction, the cross-sections plotted in Fig. 5 are based on the ldmodel 5, which uses the microscopic level densities from Hilaire's tables [39]. The present data were found in the closest agreement with the literature data. On the other hand, it can be observed in Fig. 6, the ldmodel 1 (CTFGM) as well as ldmodel 6 (temperature dependent HFB, Gogny force) were found to be in good agreement with the literature data from Ditroi et al. [9,11] and the present data for ^{89g}Zr reaction residue. As discussed earlier, the PE process can also be a channel towards the formation of the reaction residues. Therefore to calculate the precise pre-equilibrium contribution, exciton model [41] was used with the exciton number $n = 3$ which is set as default in the model code for the proton-induced reactions. However, the compound reaction results were calculated by switching off the pre-equilibrium calculations. A detailed discussion is provided in the following section.

4.2. Excitation functions of the ^{93}Nb$[(p,n),(p,pn),(p,\alpha n)]$ *reactions*

4.2.1. The ^{93}Nb$(p,n)^{93m}$Mo *reaction*

The present measured cross-section data along with the available literature data are shown in Fig. 7–9. The data have also been compared with the theoretically calculated cross-sections.

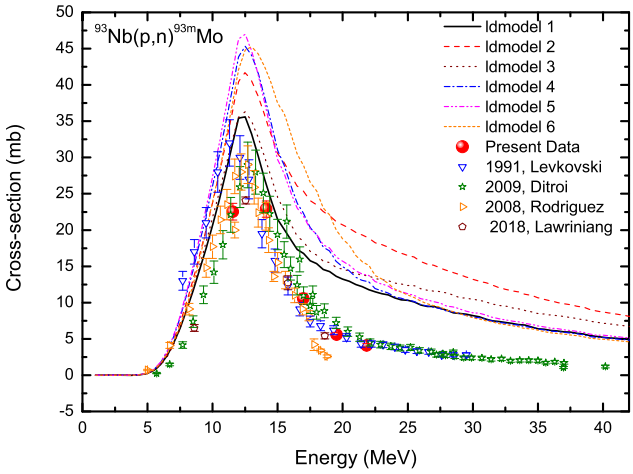

Fig. 4. (Color online.) Excitation function of the ^{93}Nb$(p, n)^{93m}$Mo reaction. The comparison of the present and the literature data [9–13,23] with different level density model parameters in TALYS-1.9 [24].

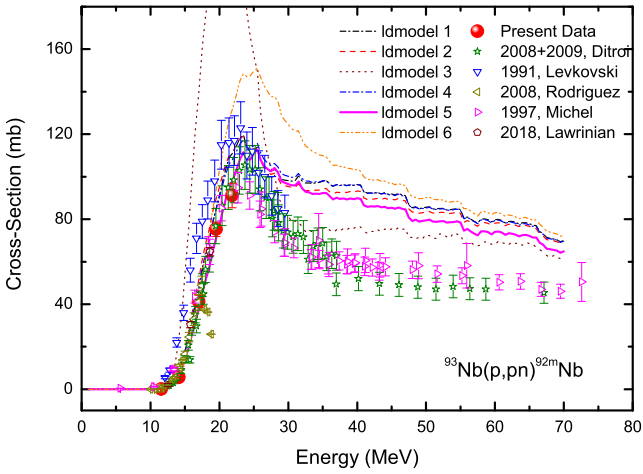

Fig. 5. Excitation function of the ^{93}Nb$(p, pn)^{92m}$Nb reaction. Rest is the same as in Fig. 4.

From the Fig. 7, it can be observed that the measured cross-sections are consistent with the literature data [9–12,23] from EXFOR [3]. It can also be found that the data from Avila Rodriguez et al. [10], Ditroi et al. [9,11] and Levkovski [12] are not consistent with each other for the incident proton energies below 14 MeV. Since the measurement is strongly dependent on the flux, therefore, the discrepancies of such an order can arise from the variation of proton flux values from the monitor reactions. However, the data from Lawriniang et al. [23] and the measured data from present work were found to be in consensus with the data from Ditroi et al. [9,11] in this energy region. Although for the energies above 16 MeV, the literature data were found consistent with each other. The default values from TALYS-1.9 model code [24] were found to be higher than the experimental data by order of magnitude. A better agreement was found when the theoretical calculations were done using exciton model as shown in Fig. 7. Furthermore, the theoretical

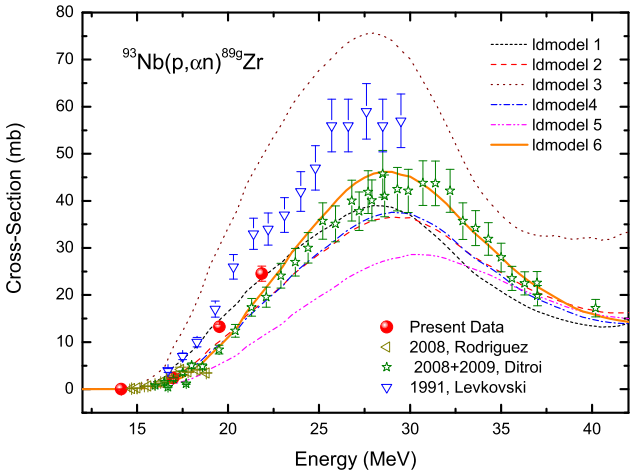

Fig. 6. (Color online.) Excitation function of the ^{93}Nb$(p, \alpha n)^{89g}$Zr reaction. Rest is the same as in Fig. 3.

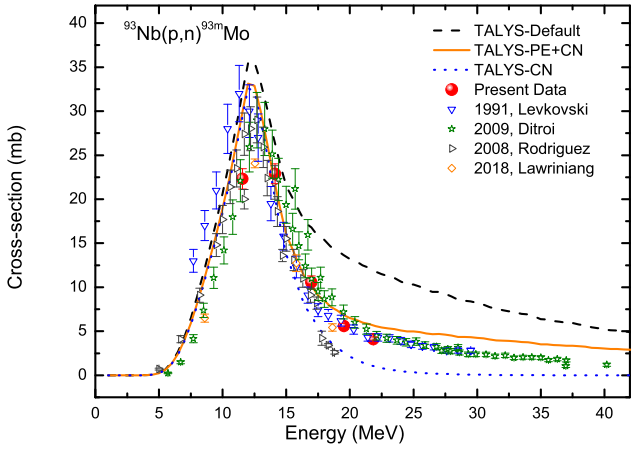

Fig. 7. Excitation function of the ^{93}Nb$(p, n)^{93m}$Mo reaction. The comparison of the literature data [9–13,23] with pure CN and CN+PE reaction cross-sections from TALYS-1.9 [24].

cross-sections using pure compound nucleus (CN) model calculations were also plotted in Fig. 7, which indicates a significant contribution from the PE reaction in the present case for incident proton energies above 15 MeV. Beyond 15 MeV the PE contribution reduces as indicated by the under estimation of the experimental results.

4.2.2. The ^{93}Nb$(p, pn)^{92m}$Nb *reaction*

The excitation function for the ^{93}Nb$(p, pn)^{92}$Nb reaction is presented in Fig. 8. From the figure, it can be observed that the literature data from Ditroi et al. [9,11], Michel [13] and Lawriniang et al. [23] are in agreement with each other in the entire energy range besides the small discrepancies in the data because of the selection of different monitor reactions and the relative uncertainties. Although, the cross-section values from Levkovski [12], were found to be slightly enhanced as observed in the previous case also. However, the cross-sections from

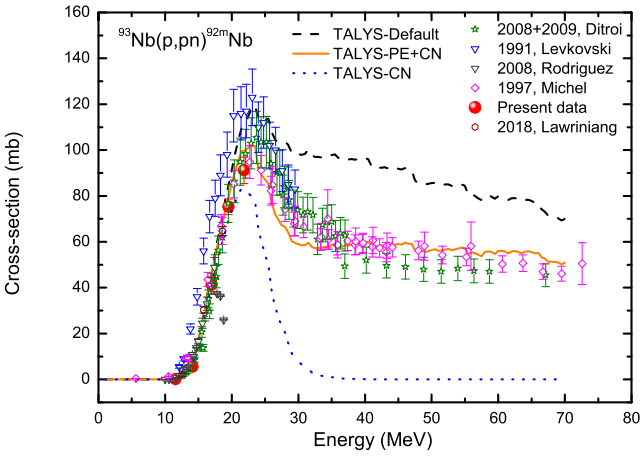

Fig. 8. Excitation function of the ^{93}Nb$(p, pn)^{92m}$Nb reaction. Rest is the same as in Fig. 6.

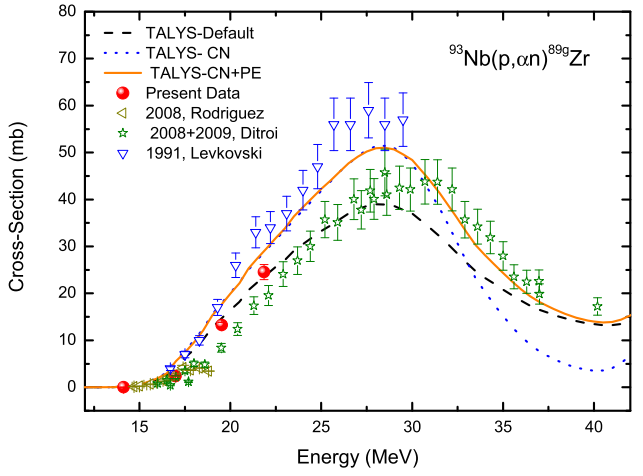

Fig. 9. (Color online.) Excitation function of the ^{93}Nb$(p, \alpha n)^{89g}$Zr reaction. Rest is the same as in Fig. 6.

Table 2
The experimental cross-sections of the (p, n), (p, pn) and $(p, \alpha n)$ reactions.

Projectile energy (MeV)	Cross-section (mb)		
	^{93}Nb$(p, n)^{93m}$Mo	^{93}Nb$(p, pn)^{92m}$Nb	^{93}Nb$(p, \alpha n)^{89g}$Zr
11.59 ± 0.46	22.31 ± 1.16	0.113 ± 0.006	–
14.13 ± 0.40	22.89 ± 1.12	5.56 ± 0.25	0.023 ± 0.002
16.98 ± 0.35	10.54 ± 0.75	41.36 ± 2.93	2.83 ± 0.18
19.53 ± 0.32	5.58 ± 0.32	75.25 ± 3.37	13.24 ± 0.59
21.85 ± 0.29	4.09 ± 0.27	91.17 ± 5.74	24.54 ± 1.59

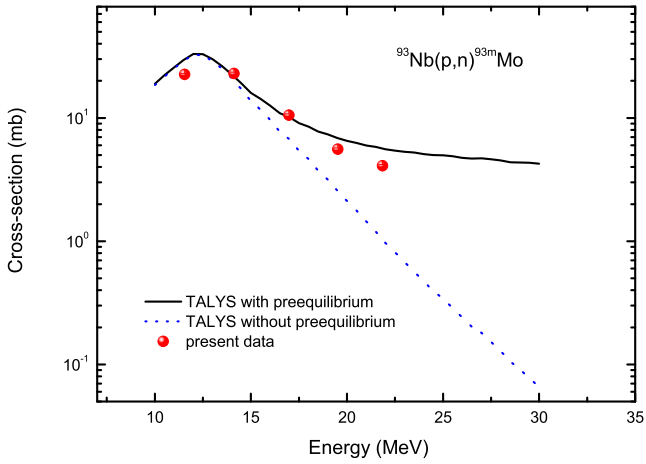

Fig. 10. (Color online.) The comparison of the present data with pure CN and CN+PRE reaction cross-sections from TALYS-1.9 [24] for the ^{93}Nb$(p, n)^{93m}$Mo reaction.

the present calculations are consistent with the literature data and the theoretically reproduced data using the TALYS-1.9 model code [24]. It can also be noted that the modified as well as the default values from the TALYS-1.9 were found successful to reproduce the experimental cross-sections up to incident proton energies around 25 MeV. However, towards the higher proton energies above 25 MeV, the predicted cross-sections from the default TALYS-1.9 input parameters are significantly higher than the literature data [9–13,23]. As indicated in figure, a reasonable amount of PE contribution can be observed for energies above 20 MeV.

4.2.3. The ^{93}Nb$(p, \alpha n)^{89g}$Zr *reaction*

The excitation function for the ^{93}Nb$(p, \alpha n)^{89g}$Zr reaction is compared with literature as well as with the results from the TALYS-1.9 model code predictions in Fig. 9. It can be seen from the figure that the data from Levkovski [12] is quite high as compared to the data from Ditroi et al. [9, 11] and the data from the present measurements. However, the current analysis and the data from Ditroi et al. [9,11] are in a good agreement with the theoretical results of the TALYS-1.9 using default values. On the other hand, the data from Avila Rodriguez et al. [10], is unexpectedly low. In the present case, the theoretical calculations using the TALYS-1.9 model code with default parameters were found to reproduce the cross-sections for the entire proton energy range of the present investigation. In the case of ^{93}Nb$(p, \alpha n)^{89g}$Zr reaction, it was noted that both the CN and PE+CN reaction cross-sections are closer to the present results up to $\approx$ 20 MeV. However, no significant PE contribution was found in the formation of the ^{89g}Zr residue for the present case. Furthermore, the PE contribution starts to increase, which is possibly due to the opening of the (p, dt) and (p, pnt) reaction channels around 35 MeV.

To provide a more clear insight into the present work, the theoretical calculations for the pre-equilibrium reaction are provided in Fig. 10 and Fig. 11 with the data only from the present work. The TALYS-1.9 model code calculations were found to be consistent with the experimental data. It is also evident from both the figures that there is a significant contribution of PE in the formation of ^{93m}Mo and ^{92m}Nb residues. Therefore, the PE contribution (PE %) was calculated at given energy for a particular channel, which can be defined as the ratio of PE cross-section to the evaporation residue cross-section. The PE fraction (PE %) from the analysis of present

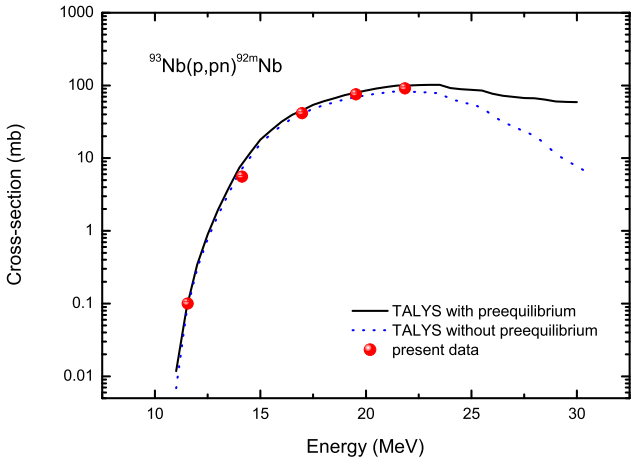

Fig. 11. (Color online.) The comparison of the present data with pure CN and CN+PRE reaction cross-sections from TALYS-1.9 [24] for the ^{93}Nb$(p, pn)^{92m}$Nb reaction.

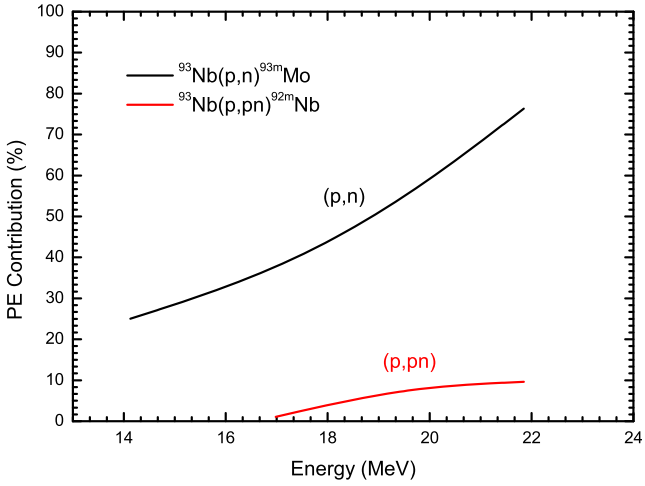

Fig. 12. (Color online.) The estimated PE contribution (PE%) from the present data as a function of projectile energy.

data for each residue are plotted in Fig. 12 as a function of incident projectile energy. As can be observed from Fig. 12, the percentage PE contribution was found to increase with the incident projectile energy. Although, the threshold for the (p, n) and (p, pn) reaction channels were found to be different, depending upon the associated Q-values. Furthermore, the PE contribution was found to be greater in the reaction that consist a single neutron in the exit channel and has a small threshold value. This may be due to the probability of single particle emission in the PE mode is higher than the multi-particle emission. It can also be stated that the PE emission inherently depends on the initial excitation energy or the Q-value of the reaction and dominate over CN formation for higher excitation energies.

5. Conclusions

In the present work, the excitation function for the ^{93}Nb[(p, n), (p, pn), $(p, \alpha n)$] reactions were experimentally determined using the stack foil activation technique at five proton energies of 21.85 ± 0.14, 19.53 ± 0.16, 16.98 ± 0.17, 14.13 ± 0.20 and 11.56 ± 0.23 MeV, respectively. The flux was measured directly from the charge integrator and current using Faraday cup instead of using monitor reaction. Different level density models have been tested in the present case. The present results were found to be in good agreement with the literature data and the theoretical calculations using the model code TALYS-1.9. The PE contribution in the ^{93}Nb(p, n) reaction was found larger than the ^{93}Nb(p, pn) reaction. This is due to the fact that there is a high probability of the emission of a single particle in PE mode. In case of the present work, TALYS-1.9 model code predictions were found successful to reproduce the cross-section data to an acceptable degree. It is necessary to mention that, the calculation of PE contribution is essential for the proton/neutron induced reactions at such higher energies. The data from the present work will be useful for the development of the future reactors, medical accelerators and to measure the dose rates for the medical isotope ^{89}Zr. The present work also serves a purpose to the use of $p + ^{93}$Nb as the monitor reaction from threshold to 22 MeV proton energies.

Acknowledgements

One of the authors (SM) thanks to the DAE-BRNS for the sanction of a major research project (Sanction Number: 36(6)/14/22/2016-BRNS) as well as providing fellowship to the author (SP). The authors are thankful to Prof. V. Nanal, Mr. Anil Shanbhag and the staffs of the Pelletron facility TIFR, Mumbai for their excellent operation of the accelerator and other supports during the experiment.

References

[1] H. Padamsee, RF Superconductivity for Accelerators, John Wiley & Sons, 1998.
[2] U. Fischer, P. Batistoni, E. Cheng, R.A. Forrest, T. Nishitani, in: Proc. International Conference on Nuclear Data for Science and Technology, vol. 769, in: AIP Conf., 2005, pp. 1478–1485.
[3] IAEA-EXFOR experimental nuclear reaction data base, http://www.nds.iaea.org/exfor.
[4] J.P. Blaser, F. Boehm, P. Marmier, P. Scherrer, Helv. Phys. Acta 24 (1951) 24.
[5] C.W. Forsthoff, R.H. Goeckermann, R.A. Naumann, Phys. Rev. 90 (1953) 1004.
[6] R.A. James, Phys. Rev. 93 (1954) 288.
[7] B.G. Kiselev, N.R. Faizrakhmanova, in: Conf. Nucl. Spectr. Nucl. Struct., Kharkov, 1974, p. 356.
[8] B.P. Singh, M.K. Sharma, M.M. Musthafa, H.D. Bhardwaj, R. Prasad, Nucl. Instrum. Methods A 562 (2006) 717.
[9] F. Ditrói, S. Takács, F. Tárkányi, M. Baba, E. Corniani, Y.N. Shubin, Nucl. Instrum. Methods B 266 (2008) 5087.
[10] M.A. Avila-Rodriguez, J.S. Wilson, M.J. Schueller, S.A. McQuarrie, Nucl. Instrum. Methods B 266 (2008) 3353.
[11] F. Ditró, A. Hermanne, E. Corniani, S. Takács, F. Tárkányi, J. Csikai, Y.N. Shubin, Nucl. Instrum. Methods B 267 (2009) 3364.
[12] V.N. Levkovski, Activation Cross Sections by Protons and Alphas, Inter-Vesi, Moscow, 1991.
[13] R. Michel, R. Bodemann, H. Busemann, R. Daunke, M. Gloris, H.J. Lange, B. Klug, A. Krins, I. Leya, M. Lüpke, S. Neumann, H. Reinhardt, M. Schnatz-Büttgen, U. Herpers, T. Schiekel, F. Sudbrock, B. Holmqvist, H. Condé, P. Malmborg, M. Suter, B. Dittrich-Hannen, P.W. Kubik, H.A. Synal, D. Filges, Nucl. Instrum. Methods B 129 (1997) 153.
[14] A. Yadav, P.P. Sing, M.K. Sharma, D.P. Singh Unnati, B.P. Singh, R. Prasad, M.M. Musthafa, Phys. Rev. C 78 (2008) 044606.
[15] H. Feshbach, Rev. Mod. Phys. 46 (1974) 1.
[16] H. Ejiri, et al., Nucl. Phys. A 305 (1978) 167.
[17] E. Gadioli, E. Gadioli-Erba, J.J. Hogan, B.V. Jacak, Phys. Rev. C 29 (1984) 76.

[18] J. Ernst, et al., Z. Phys. A 328 (1987) 333.
[19] I.A. Rizvi, K. Kumar, T. Ahmad, A. Agarwal, A.K. Chaubey, Indian J. Phys. 86 (10) (2012) 913–918.
[20] M. Blann, Phys. Rev. Lett. 27 (1971) 337, Phys. Rev. Lett. 27 (1971) 700 (Erratum).
[21] M. Blann, Phys. Rev. Lett. 28 (1972) 757.
[22] M. Blann, Code ALICE-91 PSR-146, Statistical Model Code System with Fission Competition, Oak Ridge National Laboratory, Peripheral Shielding Routine Collection, Lawrence Livermore National Laboratory and IAEA, Livermore, 1991.
[23] B. Lawriniang, R. Ghosh, S. Badwar, V. Vansola, Y.S. Sheela, S.V. Suryanarayana, H. Naik, Y.P. Naik, B. Jyrwa, Nucl. Phys. A 973 (2018) 79–88.
[24] A.J. Koning, S. Hilaire, S. Goriely, TALYS user manual, A nuclear reaction program, NRG-1755 ZG PETTEN, The Netherlands, 2015.
[25] H. Kumar, S.A. Tali, M.A. Ansari, D. Singh, R. Ali, K. Kumar, N.P.M. Sathik, S. Parashari, A. Ali, R. Dubey, I. Bala, R. Kumar, R.P. Singh, S. Muralithar, Nucl. Phys. A 960 (2017) 53–77.
[26] S.A. Tali, H. Kumar, M.A. Ansari, A. Ali, D. Singh, R. Ali, P.K. Giri, S.B. Linda, S. Parashari, R. Kumar, R.p. Singh, S. Muralithar, Nucl. Phys. A 970 (2018) 208–223.
[27] J.F. Ziegler, Nucl. Instrum. Methods B 219 (2004) 1027, http://www.srim.org/.
[28] NuDat 2.7β 2011, National Nuclear Data Center, Brookhaven National Laboratory, http://www.nndc.bnl.gov/.
[29] Qtool: calculation of reaction Q-values and threshold, Los Alamos National Library, http://cdfe.sinp.msu.ru/services/calc_thr/calc_thr.html.
[30] R. Makwana, S. Mukherjee, P. Mishra, H. Naik, N.L. Singh, M. Mehta, K. Katovsky, S.V. Suryanarayana, V. Vansola, Y.S. Sheela, M. Karkera, R. Aharya, S. Khirwadkar, Phys. Rev. C 96 (2017) 024608.
[31] R. Capote, et al., Nucl. Data Sheets 110 (2009) 3107.
[32] A.J. Koning, J.P. Declaroche, Nucl. Phys. A 713 (2003) 231.
[33] W. Hauser, H. Feshbach, Phys. Rev. 87 (1952) 366.
[34] C. Kalbach, Phys. Rev. C 33 (1986) 818.
[35] A. Gilbert, A.G.W. Cameron, Can. J. Phys. 43 (1965) 1446.
[36] W. Dilg, W. Schantl, H. Vonach, M. Uhl, Nucl. Phys. A 217 (1973) 269.
[37] A.V. Ignatyuk, K.K. Istekov, G.N. Smirenkin, Sov. J. Nucl. Phys. 29 (4) (1979) 450.
[38] A.V. Ignatyuk, J.L. Weil, S. Raman, S. Kahane, Phys. Rev. C 47 (1993) 1504.
[39] S. Goriely, S. Hilaire, A.J. Koning, Improved microscopic nuclear level densities within the HFB plus combinatorial method, Phys. Rev. C 78 (2008) 064307.
[40] S. Hilaire, M. Girod, S. Goriely, A.J. Koning, Temperature dependent combinatorial level densities with the D1M Gogny force, Phys. Rev. C 86 (2012) 064317.
[41] A.J. Koning, M.C. Duijvestijn, A global pre-equilibrium analysis from 7 to 200 MeV based on the optical model potential, Nucl. Phys. A 744 (2004) 15.